



HAL
open science

Dislocations imaging in low boron doped diamond epilayers using Field Emission Scanning Electron Microscopy (FE-SEM)

Cyrille Barbay, Samuel Saada, Christine Mer, S. Temgoua, J. Barjon,
Jean-Charles Arnault

► **To cite this version:**

Cyrille Barbay, Samuel Saada, Christine Mer, S. Temgoua, J. Barjon, et al.. Dislocations imaging in low boron doped diamond epilayers using Field Emission Scanning Electron Microscopy (FE-SEM). Applied Surface Science, 2019, 495, pp.143564. 10.1016/j.apsusc.2019.143564 . hal-02976691

HAL Id: hal-02976691

<https://hal.science/hal-02976691v1>

Submitted on 20 Dec 2021

HAL is a multi-disciplinary open access archive for the deposit and dissemination of scientific research documents, whether they are published or not. The documents may come from teaching and research institutions in France or abroad, or from public or private research centers.

L'archive ouverte pluridisciplinaire **HAL**, est destinée au dépôt et à la diffusion de documents scientifiques de niveau recherche, publiés ou non, émanant des établissements d'enseignement et de recherche français ou étrangers, des laboratoires publics ou privés.



Distributed under a Creative Commons Attribution - NonCommercial 4.0 International License

Dislocations imaging in low boron doped diamond epilayers using Field Emission Scanning Electron Microscopy (FE-SEM).

C. Barbay, S. Saada, C. Mer-Calfati, S. Temgoua, J. Barjon, J. C. Arnault

Abstract

A contrast clearly correlated with the linear defect network into boron-doped diamond epilayers was evidenced by FE-SEM observations performed at 20 kV. According to this study, this effect is dependent on the incident electron energy, the boron concentration, the thickness of the epilayer and the surface termination. These contrasts are confirmed to correspond to dislocations by revealing the etch pits using a H₂/O₂ plasma and by cathodoluminescence analyses. Boron impurities seem to play a major role in the contrast formation.

Keywords: SEM imaging; defects; CVD diamond; boron doping

1. Introduction

Homoepitaxial Boron Doped Diamond (BDD) epilayers of high crystalline quality grown by Chemical Vapor Deposition (CVD) on High Pressure High Temperature (HPHT) substrates are highly required for power electronic applications [1-2]. Surfaces of HPHT substrates are typically processed by mechanical polishing inducing “secondary” dislocations in the subsurface area [3]. More defects are added to the already present dislocations usually found in the diamond bulk and created during the HPHT synthesis [4]. During CVD homoepitaxial growth, these dislocations may thread into the epitaxial doped layers [5]. These structural defects are detrimental to electronic properties of diamond devices [6]. For power devices, the drift layer plays an essential role to increase the breakdown voltage [7]. Besides its thickness and doping level, the ability of a diode or a transistor to withstand high electric fields depends strongly on the structural defect density in this lightly doped epilayer which affects both leakage current and breakdown voltage [8]. Therefore, one of the main challenges to fabricate diamond devices with high electronic performances is to reduce the dislocation density within the CVD diamond epilayers.

Different methods are regularly used to observe dislocation networks. The most common are the X-Ray white beam topography using Synchrotron facilities [6, 9-10] or the High Resolution Transmission Electron Microscopy (HRTEM) [11-13]. Cathodoluminescence (CL) imaging can also evidence structural defects when a filter in the excitonic range is used (235 nm). Indeed, dislocations appear as dark contrast on CL images as they are good non-radiative exciton recombination centers [14-16]. H₂/O₂ etching is also frequently applied to diamond epilayers to reveal the emergent dislocations and estimate the dislocation density [17]. Using the electron channeling contrast (ECC) in a scanning electron microscope (SEM), structural defects including dislocations were recently imaged in polycrystalline diamond films [18].

In this paper, we report on a non-destructive approach to visualize the linear defect network in BDD epilayers using FE-SEM. Throughout this study, we investigated the different parameters (doping

concentration, surface termination, acceleration voltage) which govern such a contrast of the structural defects in diamond.

2. Experimental procedure

Substrates used for homoepitaxy are HPHT (3x3x0.5mm³) type Ib (100) commercially provided by Sumitomo Electronic Industry. Diamond growth was performed in two different homemade metallic walls MWPACVD (Microwave Plasma Assisted Chemical Vapor Deposition) reactors, depending on the desired boron doping level ($[B] \leq 5 \times 10^{17}$ at/cm³ or $[B] > 5 \times 10^{17}$ at/cm³). Reactors are powered by 2.45 GHz microwave generators, boron atoms were incorporated in diamond epilayers using Trimethylboron (TMB, B(CH₃)₃) precursor added to the gas mixture with varied [B/C] ratio. To achieve very low boron doping, we used a dedicated MWPACVD reactor (low boron contamination) with an oxygen content of 0.5 Vol. % (known to reduce the boron incorporation [19, 20]). The growth was carried with two different CH₄/H₂ mixtures respectively (0.25 Vol.%) and (1 Vol.%). The boron ratio to carbon, in the gas phase, $[B]/[C]_{gas}$, was varied between 400 and 30000 ppm for very low and high doping level. Boron concentrations in the epilayers were determined via a calibration based on Secondary Ion Mass Spectrometry (SIMS) which behaves a detection limit of 1.7×10^{15} at/cm³ for boron and Cathodoluminescence (CL) measurements. CVD growth conditions are reported in the Table 1.

Table 1 : Growth conditions of low and high boron doped diamond films

Conditions	Low doping $\leq 5 \times 10^{17}$ at/cm ³	High doping $\geq 10^{18}$ at/cm ³
Microwave Power (W)	600	530
Pressure (mbar)	90	115
CH ₄ / H ₂ (Vol. %)	0.25	1
[O ₂]/[H ₂] (Vol. %)	0.5	0
[B]/[C] _{gas} (ppm)	400	30000
T (K)	1200	1150-1200

Prior to each growth, samples were cleaned in an acid mixture (H₂SO₄+KNO₃) oxidizing the surface. This first step was followed by an *in situ* H₂ plasma for 30 min, under the same conditions of microwave power and pressure than the growth itself. Similar conditions were used to hydrogenate/oxidize the surface of diamond specimens for studying the influence of surface termination on the SE contrast.

CVD diamond epilayers were characterized with a Field Emission Scanning Electron Microscope (FE-SEM) ZEISS SUPRA 40 equipped with an in-lens detector which is sensitive to secondary electrons (SE) (mainly direct secondary electrons (SE1) with a small contribution of SE2, secondary electrons produced by backscattered electrons). Cathodoluminescence spectroscopy was performed under a 7 kV electron beam produced in a 7001F scanning electron microscope with field emission gun. At this voltage, the stopping depth of electrons in diamond is about 400 nm [21]. The intensity of the electron beam was set to 22 nA, measured with a Faraday cup. The samples were cooled down at 80 K thanks to a cold finger using liquid helium.

3. Results and discussion

a. SEM imaging of defects in diamond boron-doped epilayers: involved parameters

Influence of the acceleration voltage

A 1 μm thick BDD epilayer with low boron concentration (close to $5 \cdot 10^{15}$ at/cm^3) was deposited. Then, its surface was hydrogenated as described in part 2. Fig. 1 shows the FE-SEM images of the hydrogenated epilayer using the in-lens detector and two different accelerating voltages for the primary electrons (E_0): 1kV and 20 kV.

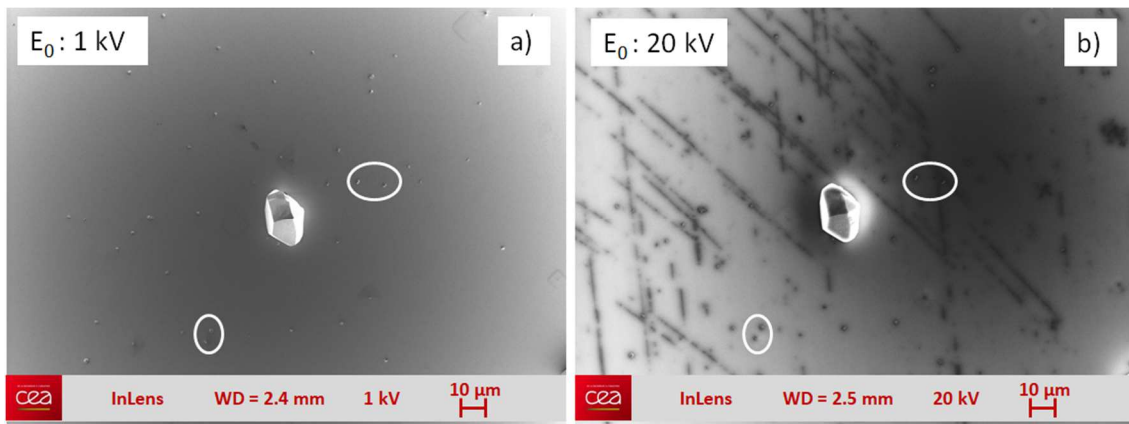


Figure 1 : FE-SEM images of the same area of a diamond boron-doped epilayer recorded at 1 kV and 20 kV, white circles highlight small non-epitaxial crystallites

At 1kV (Fig. 1a), a non-epitaxial crystallite is observed at the center surrounded by smaller non-epitaxial crystallites. The same area observed at 20 kV reveals dark lines and dark spots with some correlated to the position of non-epitaxial crystallites. However, no visible feature at 1kV could be correlated to the dark lines observed at 20 kV. The dark lines appear from an acceleration voltage of 10 kV and the contrast between dark lines and the background increases with the electron beam voltage. Tatsumi et al. have previously observed and associated dark areas observed by SEM to crystalline defects [22]. They correlated this contrast to the electron trapping by defects on hydrogenated surface. Contrary to lower electron energy which highlights the surface morphology, the electron interaction volume is bigger at high energy, probing deeper in the material, deeper than 2.5 μm according to Monte-Carlo simulations [23].

Another hypothesis considers the SE1/SE2 ratio collected by the in-lens detector coupled with the fact that SE2 emission is correlated to backscattered electrons (BSE) contrast [24]. The in-lens detector of the ZEISS SUPRA 40 microscope is mainly sensitive to SE1 but there is also a small contribution of SE2. SE2 are emitted by BSE which are sensitive to the atomic number of atoms. At low acceleration voltage, the SE1 contribution is the major one, the contribution of SE2 is very weak because the penetration depth of the beam is reduced. At higher voltage acceleration, penetration depth increases and more BSE are generated which induce more SE2. In these conditions, one can

suppose that the ratio of SE1/SE2 is decreasing according to the voltage acceleration. Consequently, the contrast associated to atomic number is increasing with the SE2 contribution. Indeed, SE2 are related to BSE contrast which is directly associated to the boron and carbon atoms distribution. Moreover, we observed that this contrast is visible at voltage higher than 10 kV and increases with the acceleration voltage. However, the atomic number of carbon is very close to boron, but this may be compensated by the in-lens detector sensitivity.

Following this fact, the several black lines and spots revealed at 20 kV are suggested, due to their arrangement, to be structural defects. These defects could be generated from polishing process which threaded into the diamond epilayer or defects which are located below the growth interface and revealed only at high voltage because in this case, the thickness of the layer is lower than the probed thickness at 20 kV.

The same phenomenon is observed with imaging technique such as cathodoluminescence (CL), this aspect will be developed in detail in section b. To make sure this contrast originates from the actual defects, a H₂/O₂ plasma etching was applied to the sample. It is known that such method enables to etch preferentially the defects due to its high anisotropy, leaving squared-etch pits on the surface [17]. The conditions used for H₂/O₂ plasma were a microwave power of 800W, a pressure of 133 mbar and 25 vol. % of O₂ diluted in H₂ for 20 min at 1273 K, the etching depth is estimated to 0.8 μm by weight measurement method. Figure 2 displays FE-SEM images of the surface before and after etching. The electron beam energy used for the second image was taken at 1 kV to probe the extreme surface and highlight the surface topography. Consequently, it demonstrates that the dark lines observed correspond to the linear defect network since the etch pits are located at the same positions than the black contrasts. According to previous report [17], these contrasts well correlate with emergence points of dislocations at the surface.

However, the H₂O₂ plasma revealed a few etch pits in areas where no contrast was observed by FE-SEM. Most of them are isolated and not adjacent to the lines. The SE contrast might be insufficient to observe the emergence of unitary dislocations, while the intersection of dislocations closely packed with the surface along a line are detected.

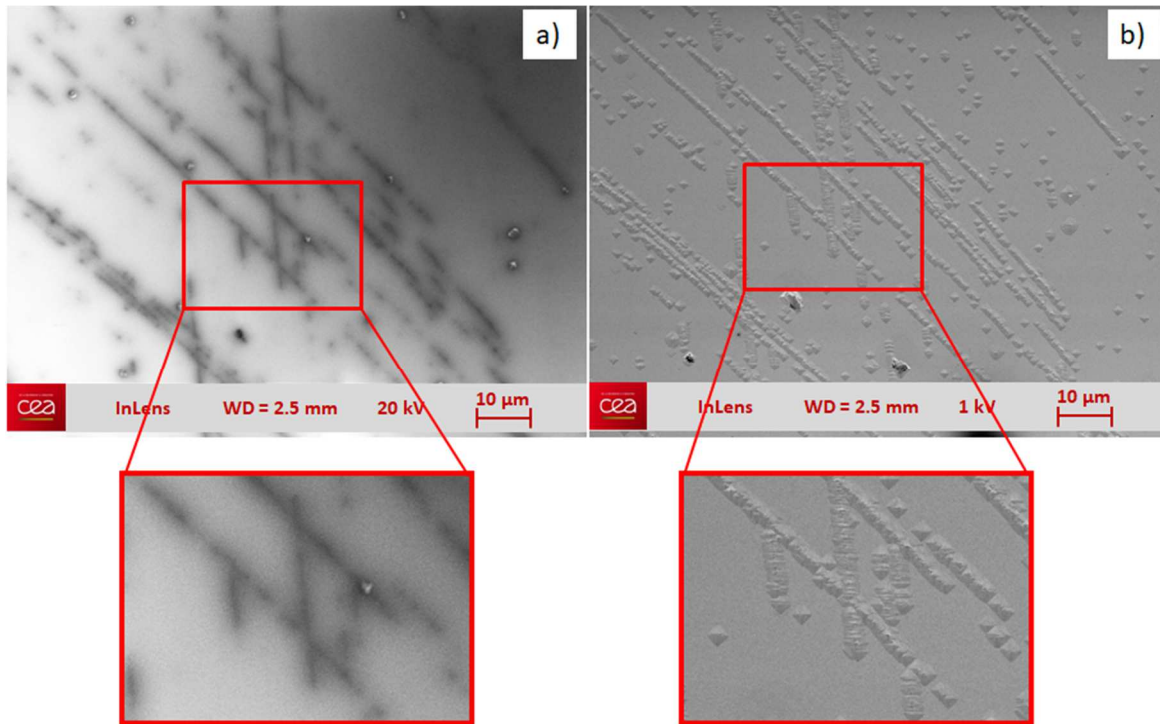


Figure 2 : FE-SEM images performed on the same area of a diamond boron-doped layer a) at 20 kV b) at 1 kV after H₂/O₂ plasma etching

Influence of the surface termination

Subsequently, we investigated the effect of surface termination on the observed contrasts. FE-SEM imaging was performed on the same area of a boron doped diamond layer ($5 \times 10^{15} \text{ at/cm}^3$) with a thickness of $1.5 \mu\text{m}$ either upon acid cleaning (oxidizing) or after hydrogen plasma (hydrogenating) (Figure 3). As a result, no contrast could be seen at 20 kV on the oxidized surface whereas a clear contrast appeared on the hydrogenated one. Hydrogen-terminated diamond surfaces exhibit unique electronic properties. Indeed, contrary to oxidized surfaces, these surfaces behave a negative electron affinity i. e. the conduction band minimum is located above the vacuum level which favors the extraction of electrons from the conduction band to the vacuum [25]. Additionally, it was shown that BDD epilayers with H-terminated surface display a secondary-electron yield nearly three times higher than after a simple acid cleaning [26]. Therefore the hydrogenation of the diamond epilayer surface is thus required to image the defects.

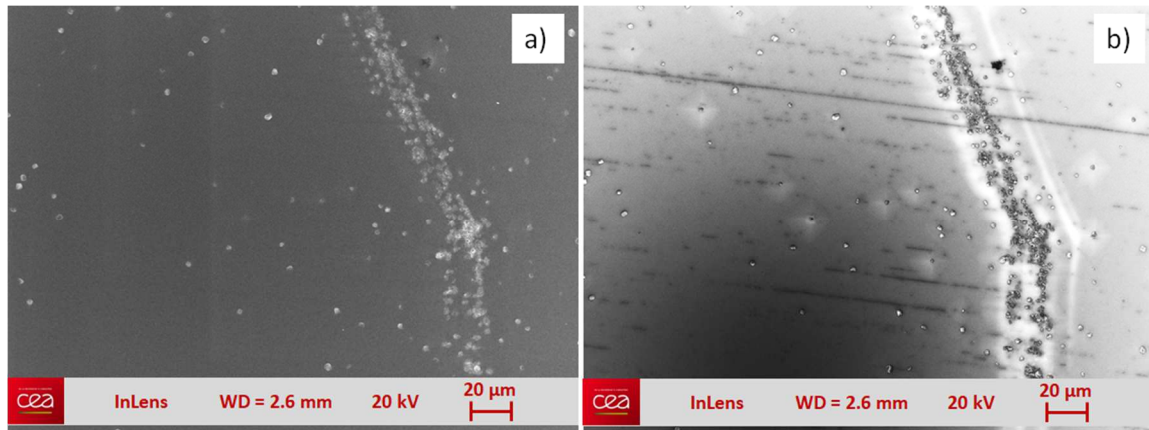


Figure 3 : FE-SEM images performed on the same area of a diamond boron-doped epilayer a) after acid cleaning b) after H₂ plasma

Influence of the epilayer thickness

The epilayer thickness has also an effect on the observed contrast. An epilayer with a boron concentration estimated to $5 \cdot 10^{15}$ at/cm³ was grown sequentially to achieve successive thicknesses (100, 200, 550, 750 and 1150 nm). Each thickness was calculated by weight difference before and after growth. The same area of the hydrogenated epilayer surface was imaged by SEM at 20 kV after each growth. No contrast was observed after the two first depositions. Black lines started to be visible after the third growth step, for a thickness superior or equal to 550 nm. As discussed below, the boron atoms are involved in the contrast origin, so we can reasonably infer that the thicker the layer is, the higher is the probability of the secondary electron to interact with boron or defects induced by the presence of boron. So, the origin depth of SE is also a key parameter to obtain this contrast and must be higher than 550 nm.

Influence of boron doping

Several substrates with epilayers (thicknesses included between 1 to 1.5 μm) of different boron concentrations according to SIMS analyses (ranging from $5 \cdot 10^{15}$ to $2 \cdot 10^{20}$ at/cm³) have been characterized by FE-SEM (Table 2). The working distance was kept at 2.5 mm, brightness and contrast at respectively 50 % and 25 %. At $E_0 = 20$ kV, no defects network have been observed at a boron concentration over $1 \cdot 10^{17}$ at/cm³. Similarly, when no boron incorporation was involved (as-received substrate or intrinsic layer), no contrast of defects appeared. Hence, it seems the presence of boron atoms in the diamond lattice has a significant part in the contrast origin. At low concentration, the boron segregation on structural defects like dislocations can play a significant role while at high concentration the boron incorporation is more homogeneous in the epilayer leading to the loss of the contrast.

Table 2 : FE-SEM contrast observation at 20 kV on several CVD epilayers doped with different boron concentrations

Substrate	Epilayer thickness	[B] (at/cm ³)	Contrast observed
1	-	Intrinsic	No
2	1 μm	$5 \cdot 10^{15}$	Yes
3	1.3 μm	$5 \cdot 10^{16}$	Yes
4	1.5 μm	$1 \cdot 10^{17}$	Yes
6	1.4 μm	$2 \cdot 10^{20}$	No

On the other hand, it is known that the initial crystalline quality of the substrate and the CVD growth conditions can have a significant impact on the propagation of the dislocations [27-28]. Two successive epilayers with different boron concentrations were grown on the same substrate to confirm that the boron concentration has a decisive role in the observation of the defects. On one HPHT Ib (100) substrate from Sumitomo was grown a first layer with a thickness of 0.8 μm and a high boron level of $3 \times 10^{20} \text{ at/cm}^3$. As expected, the FE-SEM observation did not show any contrast (Fig. 4). A second growth of an epilayer, 0.4 μm thick, with lower boron doping of $5 \times 10^{15} \text{ cm}^{-3}$ was performed on the same substrate. Images highlighted dark lines with a pattern that is characteristic of mechanical polishing features which means that structural defects from the substrate threaded into the low boron-doped epilayer (Fig. 4). Based on this observation, the defects which were present in the highly BDD layer were not observable. Consequently, it is demonstrated that the dark contrast corresponds to structural defects which thread into epilayers, not to defects from the HPHT substrate. Moreover, a given doping range (5×10^{15} - $1 \times 10^{17} \text{ at/cm}^3$) is required to observe the defect network.

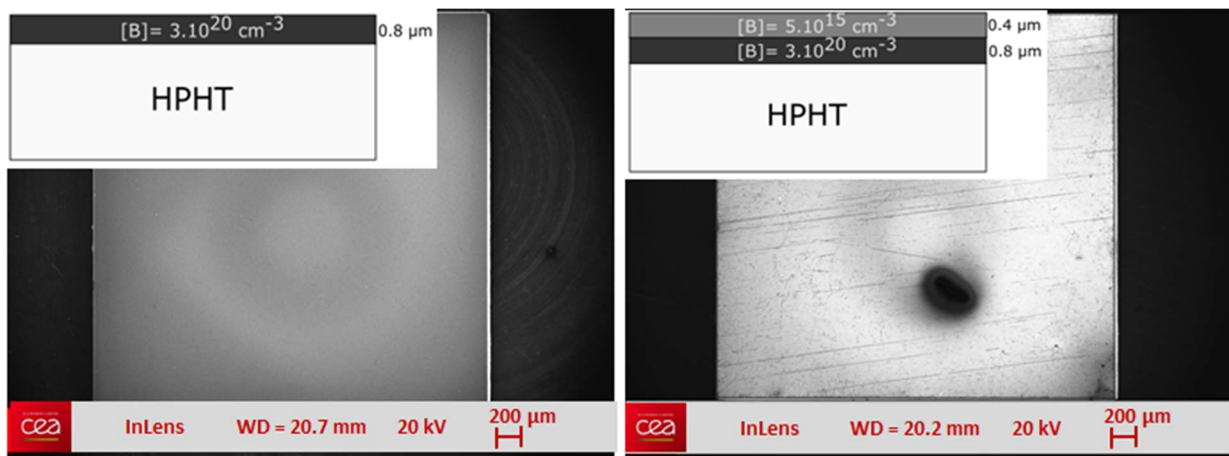


Figure 4 : FE-SEM images at 20 kV of a) high boron-doped diamond epilayer b) low boron-doped diamond epilayer grown on the same HPHT substrate. (The dark spot in the bottom right corresponds to a contamination)

b. Investigation of the contrast effect : boron concentration

It was previously shown that the electron energy, the surface termination, the epilayer thickness and the boron concentration have an influence on the contrast revealed by FE-SEM. As we delimited the doping concentration range required to observe defect contrasts, the effect of boron on the average grey level on FE-SEM images was also investigated. Four epilayers of different boron concentrations measured by SIMS were analyzed separately using the FE-SEM at 20kV. The working distance (2.5 mm), the magnification ($\times 100$), the contrast (25%) and the brightness (50%) were carefully kept constant during FE-SEM imaging.

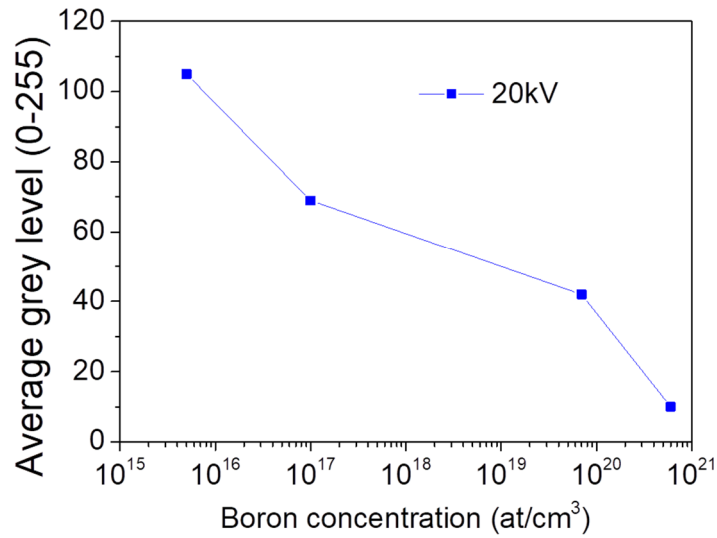


Figure 5 : Influence of the boron concentration on the average grey level of FE-SEM images

The average grey level of each image taken at the center of the samples (700x700 μm^2) was measured using *Image J* software and was plotted against the boron concentration (Figure 5). The average grey level is correlated to the secondary electron emission yield and gives a qualitative evolution of the secondary electron emission yield in a first approach. It decreases and gets darker by increasing the amount of boron atoms in the epilayer. It is assumed that the high impurity level in the material will decrease the electron escape depth and the secondary electron yield due to the higher probability for low-energy secondary electrons to encounter energy-losses from electron-phonon and electron-impurity scatterings [29].

As the defects appear darker on the FE-SEM images at 20 kV, it could suggest defects contain locally more boron atoms than the average concentration measured for the BDD epilayer. This may provide locally more traps for carriers. Turner et al. evidenced by HRTEM and spatially resolved electron energy-loss spectroscopy (STEM-EELS), an enrichment of boron in dislocations for heteroepitaxial diamond. It was suggested that the tensile strain near dislocations favors the incorporation of substitutional or interstitial boron atoms in the surrounding diamond lattice [12]. From this consideration, a minimal boron concentration may be necessary to induce a contrast in FE-SEM images. Nevertheless, for values over 2×10^{18} at/cm³, boron atoms could be dispersed more homogeneously over the epilayer, the segregation of boron in the defects becoming negligible.

To investigate such boron enrichment, cathodoluminescence (CL) mapping was led on a sample with an average acceptor concentration measured at 4×10^{17} cm⁻³ [30]. Several zones were observed by CL and SEM at 20 kV.

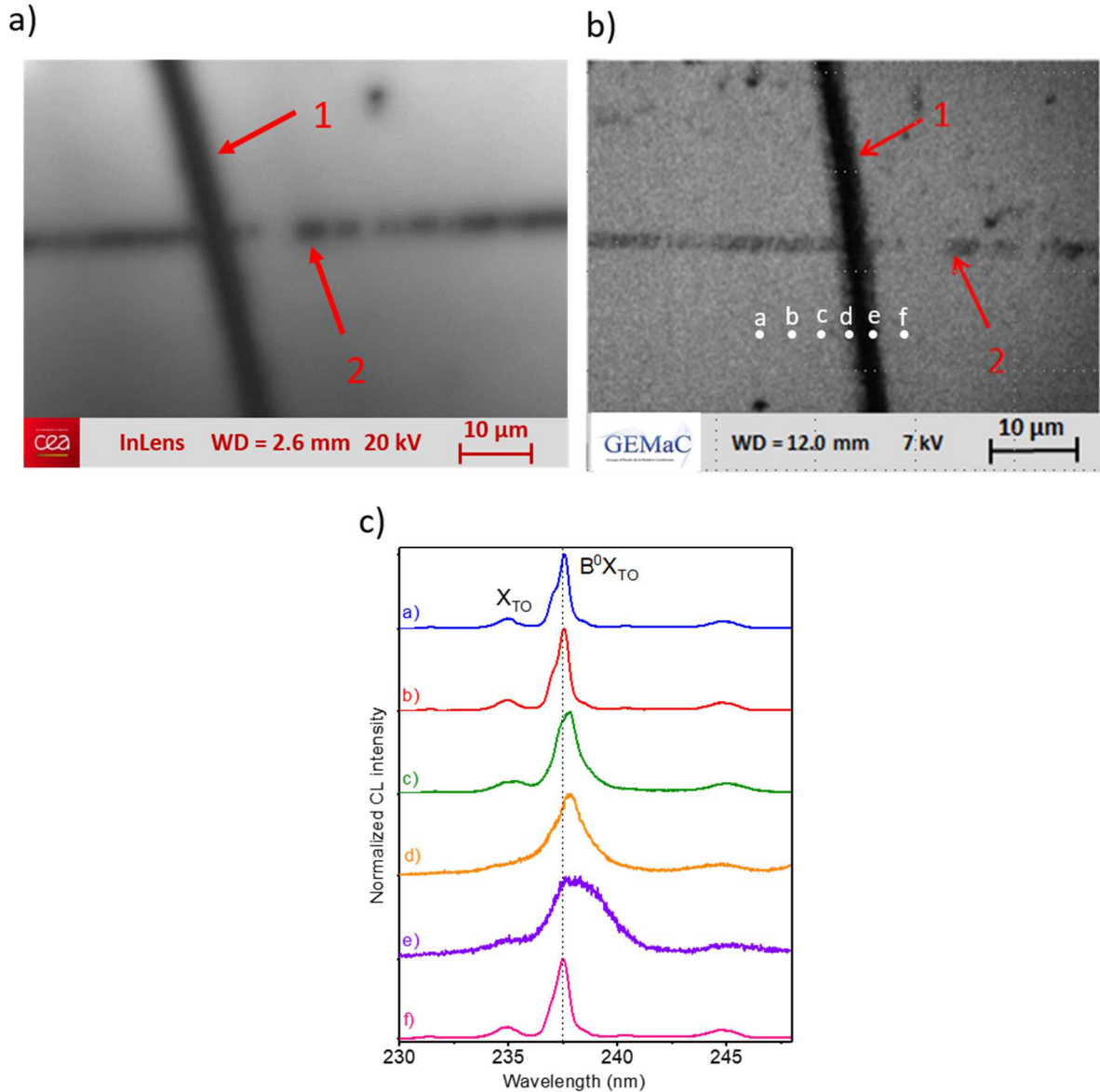


Figure 6 : Zone of a BDD epilayer, 2.7 μm thick, with an acceptor concentration of $4 \times 10^{17} \text{ cm}^{-3}$ imaged by a) FE-SEM at 20 kV; b) CL image at 235 nm; c) CL spectra recorded at some regions near dislocations.

By comparing FE-SEM image recorded at 20 kV and CL image for the same zone (Fig. 6, panels a and b), contrasted lines appear at the same position. Knowing that the black lines on the CL image filtered at 235 nm (free exciton X_{TO}) correspond to dislocations within the epilayer [16], it is stated that the defects evidenced on FE-SEM image are also dislocations. Therefore, at high voltage using FE-SEM, CL observations confirm that it is possible to visualize dislocations in a boron doped diamond layer with such a method.

The luminescence spectra, locally reported near dislocations are presented on figure 6c. It is firstly observed a shift of the boron bound exciton position B^0X_{TO} from its value at 237.6 nm in a strain-free layer (dot line) as we get closer to the dislocation [31]. This shift in position reveals the presence of strains in the near vicinity of the dislocation line 1, accompanied by a broadening of the B^0X_{TO} peak as seen on spectra d and e. Moreover, no significant change of the ratio B^0X_{TO}/X_{TO} is observed. These observations render difficult to precisely estimate the concentration of acceptors by CL around

dislocations. Other techniques such as chemical analysis in a STEM would be necessary to confirm the role of boron segregation at dislocations on the SE contrast.

Conclusion

The FE-SEM imaging of boron-doped diamond epilayers with an acceleration voltage of 20 kV reveals a specific contrast with black lines. This effect is not observed at 1 kV. According to H₂/O₂ plasma etching and cathodoluminescence mapping, these black lines were confirmed to be dislocations.

The contrast appearance at 20 kV also requires a hydrogenated diamond surface, boron impurities in the epilayer and a sufficient thickness for the BDD epilayer. Mechanisms involved in the contrast observation seem to be strongly related to the secondary emission current and the boron impurities contained in the diamond CVD epilayer (within a range from 5x10¹⁵ to 1x10¹⁷ at/cm³). It can be proposed that an enrichment of boron in dislocations favors trapping of the secondary electrons before they escape from the sample inducing a difference of secondary emission current. No acceptor enrichment was evidenced by CL observations. Nevertheless, scanning transmission electron microscopy and spatially resolved electron energy-loss spectroscopy coupled (STEM-EELS) with measurements of secondary emission current seem necessary to clarify the role of boron in the observed contrast.

FE-SEM demonstrated to be a fast, non-destructive and competitive method to analyze linear defect distributions in CVD BDD epilayers allowing a regular crystalline quality checking after growth.

Acknowledgement

This project has received funding from the European Union's Horizon 2020 Program under Grant Agreement No. 640947 (GREENDIAMOND). The authors would like to thank Marie-Amandine Pinault-Thaury from the Groupe d'Etude de la Matière Condensée (GEMAC) for SIMS analyses.

References

- [1] P. N. Volpe, P. Muret, J. Pernot, F. Omnès, T. Teraji, Y. Koide, F. Jomard, D. Planson, P. Brosselard, N. Dheilily, B. Vergne, S. Scharnholz, Extreme dielectric strength in boron doped homoepitaxial diamond, *Appl. Phys. Lett.* 97, 223501 (2010)
- [2] J. Isberg, J. Hammersberg, E. Johansson, T. Wikström, D. J. Twitchen², A. J. Whitehead, S. E. Coe², Geoffrey A. Scarsbrook², High Carrier Mobility in Single-Crystal Plasma-Deposited Diamond, *Science* 297, 1670-1672 (2002)
- [3] P. N. Volpe, P. Muret, F. Omnes, J. Achard, F. Silva, O. Brinza, A. Gicquel, Defect analysis and excitons diffusion in undoped homoepitaxial diamond films after polishing and oxygen plasma etching, *Diamond and Related Materials* 18, 1205-1210 (2009)
- [4] H. Sumiya and K. Tamasaku, Large Defect-Free Synthetic Type IIa Diamond Crystals Synthesized via High Pressure and High Temperature, *Jpn. J. Appl. Phys.* 51 (2012)
- [5] M. P. Gaukroger, P. M. Martineau, M. J. Crowder, I. Friel, S. D. Williams, D. J. Twitchen, X-ray topography studies of dislocations in single crystal CVD diamond, *Diamond and Related Materials* 17, 262-269 (2008)

- [6] M. Suzuki, T. Sakai, T. Makino, H. Kato, D. Takeuchi, M. Ogura, H. Okushi, S. Yamasa, Electrical characterization of diamond PiN diodes for high voltage applications, *Physical Status Solidi S* a 210, 2035–2039 (2013)
- [7] D. Zhao, C. Hu Z. Liu, H. X. Wang, W. Wang, J. Zhang, Diamond MIP structure Schottky diode with different drift layer thickness, *Diamond and Related Materials* 73, pp. 15-18 (2017)
- [8] H. Umezawa, N. Tatsumi, Y.Kato, S. Shikata , Leakage current analysis of diamond Schottky barrier diodes by defect imaging, *Diamond and Related Materials* 40, pp. 56-59 (2013)
- [9] M. Kasu, R. Murakami, S. Masuya, K. Harada, H. Sumiya, Synchrotron X-ray topography of dislocations in high-pressure high-temperature-grown single-crystal diamond with low dislocation density, *Applied Physics Express* 7, 125501 (2014)
- [10] M. Moore, S. G. Nailer, W. K. Wierzchowski, Optical and X-Ray Topographic Studies of Dislocations, Growth-Sector Boundaries, and Stacking Faults in Synthetic Diamonds, *Crystals* 6, 71 (2016)
- [11] A. Mussi, D. Eyidi, A. Shiryaev, J. Rabier, TEM observations of dislocations in plastically deformed diamond, *Phys. Status Solidi A* 210, 191–194 (2013)
- [12] S. Turner, H. Idrissi, A.F. Sartori, S. Korneychuck, Y. G. Lu, J. Verbeeck, M. Schreck, G. Van Tendeloo, Direct imaging of boron segregation at dislocations in B: diamond heteroepitaxial films, *Nanoscale* 8, 2212-2218 (2016)
- [13] B.-C. Gallhebera, O. Klein, M. Fischer, and M. Schreck, Propagation of threading dislocations in heteroepitaxial diamond films with (111) orientation and their role in the formation of intrinsic stress, *Journal of Applied Physics* 121, 225301 (2017)
- [14] H.Bensalah, I.Stenger, G.Sakr, J.Barjon, R.Bachelet, A.Tallaire, J.Achard, N.Vaissiere, K.H.Lee, S.Saada, J.C.Arnault, Mosaicity, dislocations and strain in heteroepitaxial diamond grown on iridium, *Diamond and Related Materials* 66, 188-195 (2016)
- [15] A. Tallaire, J. Barjo, O. Brinza, J. Achard, F. Silva, V. Mille, R. Issaoui, A. Tardieu, A. Gicquel, Dislocations and impurities introduced from etch-pits at the epitaxial growth resumption of diamond, *Diamond & Related Materials* 20, 875–881 (2011)
- [16] A. Tallaire, T. Ouisse, A. Lantreibecq, R. Cours, M. Legros, H. Bensalah, J. Barjon, V. Mille, O. Brinza, J. Achard, Identification of Dislocations in Synthetic Chemically Vapor Deposited Diamond Single Crystals, *Cryst. Growth Des.* 16 (5), 2741–2746 (2016)
- [17] M. Naamoun, A. Tallaire, F. Silva, J. Achard, P. Doppelt, A. Gicquel, Etch-pit formation mechanism induced on HPHT and CVD diamond single crystals by H₂/O₂ plasma etching treatment, *Physica Status Solidi A* 209, 1715–1720 (2012)
- [18] S. Kaboli, P. C. Burnley, Direct observations of crystal defects in polycrystalline diamond, *Materials Characterization* 142, 154-161 (2018).
- [19] D. Araujo, M. Kadri, M. Wade, E. Bustarret, A. Deneuveille, Excitonic emission and N- and B-incorporation in homoepitaxial CVD-grown diamond investigated by cathodoluminescence, *Physical Status Solid Sc* 2, 1336–1341 (2005).

- [20] P. N. Volpe, J. C. Arnault, N. Tranchant, G. Chicot, J. Pernot, F. Jomard, P. Bergonzo, Boron incorporation issues in diamond when TMB is used as precursor: Toward extreme doping levels, *Diamond & Related Materials* 22 136–141 (2012).
- [21] J. Barjon and K. Haenen, “Optical spectroscopy of doped diamond layers”, in *Power electronics device applications of diamond semiconductors* 1st edition. p. 154 (2018)
- [22] N. Tatsumi, K. Harano, T. Ito, H. Sumiya, Polishing mechanism and surface damage analysis of type IIa single crystal diamond processed by mechanical and chemical polishing methods, *Diamond & Related Materials* 63, 80–85 (2016)
- [23] Volpe, PhD thesis, Grenoble Alpes University, Réalisation de composants unipolaires en diamant pour l'électronique de puissance, 57 (2009)
- [24] H. Seiler, Secondary electron emission in the scanning electron microscope, *J. Appl. Phys.* 54, R1-R18 (1983)
- [25] J. Van Der Weide, Z. Zhang, P. K. Baumann, M. G. Wensell, J. Bernholc, R. J. Nemanich, Negative-electron-affinity effects on the diamond (100) surface, *Physical Review B* 50, 5803-5806 (1994)
- [26] A. Shih, J. Yater, P. Pehrsson, J. Butler, C. Hor, and R. Abrams, Secondary electron emission from diamond surfaces, *Journal of Applied Physics* 82, 1860 (1997)
- [27] A.B. Muchnikov, A.L. Vikharev, A.M. Gorbachev, D.B. Radishev, V.D. Blank, S.A. Terentiev, Homoepitaxial single crystal diamond growth at different gas pressures and MPCVD reactor configurations, *Diamond & Related Materials* 19, 432–436 (2010)
- [28] M. Hamada, T. Teraji, T. Ito, Hillock-Free Homoepitaxial Diamond (100) Films Grown at High Methane Concentrations, *Japanese Journal of Applied Physics* 44, L 216–L 219 (2005)
- [29] A. Shih, J. Yater, C. Hor, R. Abrams Natal, Secondary electron emission studies, *Applied Surface Science* 111, 251-258 (1997)
- [30] F. Omnès, P. Muret, P.N. Volpe, M. Wade, J. Pernot, F. Jomard, Study of boron doping in MPCVD grown homoepitaxial diamond layers based on cathodoluminescence spectroscopy, secondary ion mass spectroscopy and capacitance–voltage measurements, *Diamond & Related Materials* 20, 912–916 (2011)
- [31] J. Barjon, T. Tillocher, N. Habka, O. Brinza, J. Achard, R. Issaoui, F. Silva, C. Mer, and P. Bergonzo, Boron acceptor concentration in diamond from excitonic recombination intensities, *Phys. Rev. B* 83, 073201 (2011)